Electronic structure of defects and impurities in III-V nitrides: Vacancies in cubic boron nitride

V. A. Gubanov
Department of Physics, California State University at San Jose, San Jose, California 95192

Z. W. Lu, Barry M. Klein, and C. Y. Fong
Department of Physics, University of California, Davis, California 95616-8677

(Received 2 June 1995)

The electronic structures of boron and nitrogen vacancies in cubic boron nitride (BN) are investigated using the full-potential linearized augmented-plane-wave, full-potential linear-muffin-tin-orbital, and linear-muffin-tin-orbital–tight-binding approaches. All the methods give quantitatively consistent results on ideal cubic BN that are also compared with previous calculations. Using a 64-atom supercell, we have examined the electronic states of boron and nitrogen vacancies. Lattice relaxation around the vacancies is not considered. Both boron and nitrogen defect states appear to form well-defined narrow bands in the forbidden gap of *c*-BN. The ones for boron vacancy are located near the top of the valence band and are partially occupied. They represent ''acceptor levels of boron vacancy.'' For the nitrogen defect, the ''vacancy levels'' overlap with the states at the conduction-band edge. The characteristics of vacancy states, their localization degrees and influence on the electronic density of states, and charge distribution in *c*-BN crystals are discussed. These results suggest that both boron and nitrogen vacancies can be ''*p*-type'' and ''*n*-type'' doping agents, respectively, when the composition of *c*-BN deviates from ideal stoichiometry.

I. INTRODUCTION

Significant progress in growth methods of wide gap semiconductors in recent years has renewed interest in their use for electronic and optoelectronic devices.[1–3] Based on physical properties of these materials, novel devices can be fabricated and are expected to operate at high power, elevated temperatures, and at high frequency. For example, the blue-light-emitting diodes have been successfully built from gallium nitride (GaN). Other devices, such as ultraviolet laser diodes, ultraviolet light detectors, and high temperature diodes and transistors, may well be possible.

The most promising semiconductors for these unusual devices are the III-V nitrides, especially boron nitride, which has the widest heteropolar band gap among all III-V compounds (>6 eV) and possesses extreme hardness, chemical inertness, high thermal stability, and high resistivity. Therefore, BN is a potential candidate for high-temperature, radiation-resistant devices, and is also an effective material for ultrahard ceramics applications.[4,5] BN can also be used in the growth and processing of other semiconductors, such as gate dielectrics, x-ray lithography masks,[6] efficient heat-dissipating semiconductor substrates, wear-resistant coatings, and hard optical layers.

Being isoelectronic to carbon, it is not surprising that boron nitride has hexagonal (*h*-BN) (Ref. 3) and cubic (*c*-BN) (Ref. 7) phases similar to the graphite and diamond phases of carbon. BN is also known to exist in four other crystalline structures: rhombohedral (*r*-BN),[4] wurtzite (*w*-BN),[8] simple cubic,[9] and turbostratic (*t*-BN) (Ref. 10) phases. These are metastable structures, with the last two phases having been recently identified.

Among all the phases, cubic BN is the most interesting, both from technological and scientific points of view. Technologically, *c*-BN is the second hardest material known (exceeded only by diamond) and has excellent thermal conductivity. Scientifically, it is one of the wide gap semiconductors which can be easily doped to produce both *n*-type and *p*-type conductivities. However, the mechanism for exhibiting simultaneous *n*- and *p*-type conductivities is not well understood. There are suggestions that the formation of point defects (vacancies, antisite defects, and interstitials)[3,11] may be responsible. In fact, none of the nitride semiconductors form stoichiometric melts, and large deviations from stoichiometry are often observed.

Extreme conditions [pressures up to 5.5 GPa and temperatures of 1700 °C (Ref. 12)] are required for growing *c*-BN. A large variety of experimental techniques has been used to synthesize *c*-BN, especially in film form: chemical[13] and physical vapor deposition (CVD and PVD, respectively),[14–16] plasma enhanced CVD,[17–19] pulsed excimer laser ablation,[20] radio-frequency sputtering,[21] ion-assisted laser deposition,[22,23] neutralized nitrogen ion bombardment,[24] Ar ion-beam-enhanced deposition,[25] and others. It was shown that *c*-BN can be formed only by a sharp rise in temperature followed by fast quenching, which freezes in a metastable phase. This is usually achieved when the boron is sputtered, laser ablated, or evaporated, and the nitrogen is ionized to the N^+ or N^{2+} forms, and accelerated to the substrate (usually made of silicon), where it serves as an active ion to form a B-N bond. The cubic phase appears to form in rather narrow windows of specific experimental conditions of the momentum per atom transferred into the film in the ion bombardment techniques,[16,25] the energy of bombarding ions,[3] or the limited ranges of specific deposition temperatures and gas pressures.

Fourier transform infrared, electron probe microanalysis x-ray photoemission spectroscopy,[24] (XPS),[25] Auger spectroscopy,[23] transmission electron microscopy,[22] near-edge x-ray absorption fine structure,[26] and other experimen-

tal techniques have been used to characterize the composition and structure of boron nitride films. The c-BN phase is readily identified, and under the best experimental conditions considerable deviations from stoichiometry are usually observed. The N/B ratio varies significantly depending on the experimental conditions and the deposition technique [see, e.g., Refs. 24, 25, and 27]. Often the films have a tendency to be nitrogen deficient,[22,24] forming vacancies in the zinc-blende crystal lattice. Some other defects have been traced in the c-BN films, most typically, C,[24] H, or O impurities.[26] Traces of metals have also been found.[26]

Despite the clear recognition of the crucial influence of lattice defects on the physical and chemical properties of boron nitride phases, such as the value of the energy gap, conductivity, optical properties,[12,27] and thermomechanical properties (microhardness[14] and others), very little is known about the nature of the defect states. Traditional experimental techniques, such as deep level transient spectroscopy, for determining the energy states of intrinsic and doped samples appear to be ineffective for crystals with wide energy gaps and low conductivities. Electron spin resonance, thermostimulated luminescence, and thermostimulated conduction have been used to probe energy states of defects in the gap of h-BN.[28,29] Charge carrier trapping and recombination centers in graphitelike pyrolytic BN produced by gas-phase deposition have been investigated by thermally activated spectroscopy of luminescence and conduction.[30] Semiempirical calculations of the electronic structure of pyrolytic BN with vacancies stabilized by C have been performed[31] for h-BN. At the same time, first-principles electronic structure calculations for different phases of defect-free boron nitride have been carried out.[32–34] However, no *ab initio* calculations for defects have been reported.

In this paper, we present results of electronic structure calculations for simple defects in *unrelaxed* c-BN crystal lattice— isolated boron and nitrogen vacancies—and relate their influence on the optical and conduction characteristics of this material. The paper is organized as follows. In Sec. II, we present results for the electronic structure of the ideal c-BN crystal calculated with different band structure methods based on local density approximation (LDA):[35] the full-potential linearized augmented-plane-wave (FPLAPW),[36,37] full-potential linear combination of muffin-tin orbital (FPLMTO),[38] LMTO-atomic sphere approximation (ASA), and tight-binding (LMTO-ASA-TB) methods.[39,40] The purpose of these calculations is to justify our use of the LMTO-ASA-TB method for treating defect states in c-BN. Results of supercell calculations for the electronic structure of a boron vacancy and its effects on the electronic states of neighboring atoms will be discussed in Sec. III. In Sec. IV, we give a similar presentation of the results for a nitrogen vacancy. Finally, a summary will be given in Sec. V.

II. METHODS OF CALCULATIONS, MODELS, AND RESULTS OF BN IN IDEAL ZINC-BLENDE STRUCTURE

In order to test the sensitivity to the input parameters, such as the muffin-tin and the atomic sphere radii, for a simple but reliable technique for the studies of defect states in c-BN, we have carried out band calculations for the ideal zinc-blende phase of boron nitride (c-BN) using three different linearized approaches: (i) the highly precise FPLAPW method;[37] (ii) the FPLMTO method developed by Methfessel;[38] and (iii) the LMTO-ASA-TB method[39] developed recently.[40] These methods are based on the LDA,[35] for which we have used the Hedin-Lundqvist exchange-correlation form.[41]

c-BN crystallizes in the zinc-blende structure (two atoms/cell) with a lattice parameter of 3.615 Å.[42] Recent transmission electron microscopy data[20] for 1000-Å-thick films on Si substrate give a lattice parameter of 3.62 Å (with an error of $<1\%$). Therefore, a value of 3.615 Å is used in our first set of calculations. The other computational details are as follows: The muffin-tin radii were 1.42 a.u. for both B and N in the FPLAPW calculations, while in the FPLMTO calculations the muffin-tin radii were 1.479 a.u. for both B and N, and the angular momentum cutoff was $l=4$. In the FPLMTO calculations, a multiple κ muffin-tin-orbital basis set was used. Three augmented Hankel functions with decay energies κ of -0.01, -1.0, and -2.3 Ry were utilized. In order to improve the description of the potential in the interstitial region, two empty spheres (ES) at standard ($-1/4$, $-1/4$, $-1/4$) and (1/2, 1/2, 1/2) positions were used. In this LMTO-ASA-TB-ES method, the radii of the atomic and empty spheres were set equal to the Wigner-Seitz radius. The summations in reciprocal space were done using ten special **k** points[43] in the FPLAPW method.

To model an isolated vacancy in c-BN, a cubic supercell consisting of eight zinc-blende cells with 64 atoms was used. The vacancy was located at the center of the supercell and was simulated by a ''vacancy empty sphere,'' with s, p, and d vacancy states included in the orbital basis. Atoms and vacancy are located on the ideal zinc-blende sites and no structural relaxations are included in the current calculations. Using first-principles methods such as the FPLAPW or FPLMTO methods on such a big supercell is computationally prohibitive. On the other hand, a simplified approach such as the self-consistent LMTO-ASA-TB method is feasible. In an attempt to simplify the supercell calculations, we have performed a less accurate, but simplified, option in the LMTO-ASA-TB calculations — no empty sphere was introduced in the traditional way, but the degree of atomic sphere overlap was increased to fill the whole unit cell volume. We will refer to this method of such calculations as ''the LMTO-TB-NO-ES.''

Figure 1 compares the calculated band structures for c-BN using the different methods. The values for the band gap and band widths are summarized in Table I. These results are in reasonable agreement with each other: the dispersion of the bands computed by the FPLAPW and FPLMTO methods is practically indistinguishable for both the valence and the conduction bands. The band orderings at the high symmetry points are identical and the band widths are very close (Table I) and agree well with the results of an earlier FPLAPW calculation.[32] In comparing these results to the ones calculated by the LMTO-ASA-TB method [Fig. 1(c)], there are some relatively small increases in the gap values at various **k** points (Table I). The overall agreement, however, is very good. These comparisons give us confidence in using the simplified LMTO-ASA-TB method to study defect states in c-BN (Secs. III and IV).

The calculated lattice constants are listed in Table II. All

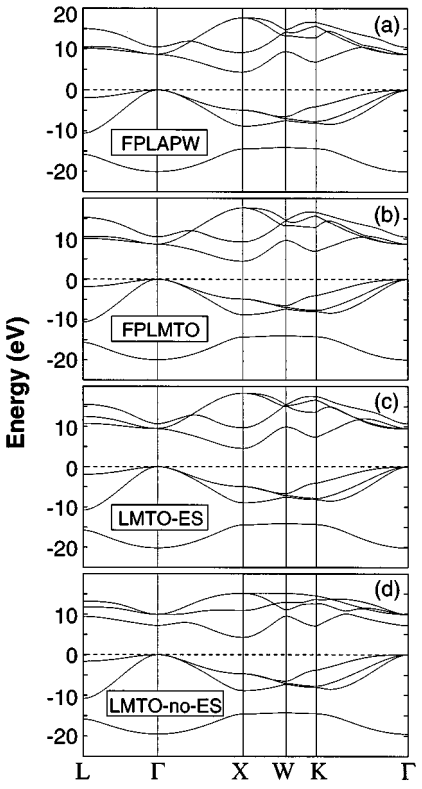

FIG. 1. Calculated energy bands for zinc-blende BN (c-BN) using the (a) FPLAPW (b) FPLMTO, (c) LMTO-ASA-ES, and (d) LMTO-ASA-NO-ES methods. The energy zero is set at the top of the valence band.

methods (except for the LMTO-TB-NO-ES) yield values of the lattice constant which are $<1\%$ smaller than the experimental value. This is typical for the LDA calculations. The ''exact'' agreement with the experimental value of the lattice constant obtained by LMTO-TB-NO-ES and by the similar method in Ref. 33 is probably fortuitous. The equilibrium bulk modulus determined by the FPLAPW method is 402 GPa which agrees reasonably well with the experimental value of 380 GPa.

TABLE II. Calculated and experimental lattice constants for c-BN.

	Present work				Expt.	Other work	
	FPLAPW	FPLMTO	LMTO-TB ES	LMTO-TB NO-ES			
a_0 (Å)	3.59	3.58	3.58	3.62	3.62	3.61 [a]	3.59 [b]

[a]LMTO-ASA, Ref. 33.
[b]FPLAPW, Ref. 32.

The charge distributions in the (110) plane obtained by the FPLAPW method are presented in Fig. 2(a). Strong ionicity of the bonding can be easily discerned, with electronic charge transferred from the boron atom to the nitrogen atom. The difference in charge density between the calculated charge density and a superposition of free-atom charge densities [Fig. 2(b)] illustrates nicely the overall strong directional B-N bonding in the (110) plane. Figure 3 depicts the charge density contours obtained from the LMTO-ASA-TB results with [Figs. 3(a) and 3(b)] and without [Figs. 3(c) and 3(d)] empty spheres. Again, both the FPLMTO (not shown here) and LMTO-ASA-TB methods (Fig. 3) provide similar descriptions of the charge density for the occupied bands to the FPLAPW method [Fig. 2(a)], while the simplified LMTO-TB-NO-ES results do not show any significant difference in the total charge density distributions either.

Figure 4 gives the total and partial densities of states (DOS) deduced from the LMTO-ASA-TB calculations (using 245 nonequivalent **k** points in the irreducible Brillouin zone). As is seen, the lower part of the valence band (between -20 and -15 eV) is formed by the N $2s$ states. The N $2p$ states hardly contribute to the bands in this energy region, but they do hybridize strongly with both $2s$ and $2p$ states of boron in the upper part of the valence bands (-11 eV and above). N $2p$ and B $2s$ hybridization is most pronounced at the bottom of the upper valence band region,

TABLE I. Energy gaps and band widths (in eV) for the zinc-blende BN. W_L, W_U, W_T denote the lower valence band width, upper valence band width, and total valence band width, respectively.

Gap widths	Present work				Other work		
	FPLAPW	FPLMTO	LMTO-TB ES	LMTO-TB NO-ES			
Γ_v-Γ_c	7.2	8.62	8.52	8.21	8.93[a]	8.8[b]	8.6[c]
Γ_v-L_c	9.4	10.25	10.57	10.42	10.29[a]		
Γ_v-X_c	4.3	4.41	4.48	4.32	4.42[a]	4.4[b]	4.2[c]
Γ_v-K_c	7.1	6.85	7.29	7.20			
W_v-W_c	16.1	16.12	16.01	16.03			
W_L	5.2	6.02	6.08	6.11		5.9[b]	5.2[d]
W_U	10.8	10.54	10.79	10.81		10.7[b]	13.5[d]
W_T	19.5	20.01	20.17	20.14		20.1[b]	22[e]

[a]LMTO-ASA, Ref. 33.
[b]FPLAPW, Ref. 32.
[c]Pseudopotential, Ref. 44.
[d]X-ray experiment, Ref. 45.
[e]XPS experiment, Ref. 46.

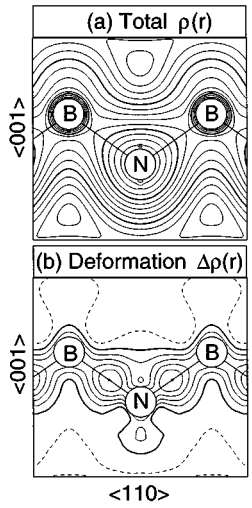

FIG. 2. Charge density distribution in the (110) plane calculated using the FPLAPW method: (a) total charge density, where successive contours differ by $\rho_{n+1}/\rho_n = 1.350$; and (b) difference charge density, where successive contours differ by $\rho_{n+1} - \rho_n = 0.08e/A^3$. A solid dark line next to a dashed line indicates the zero contour, while solid (dashed) lines indicate charge accumulation (depletion).

while the B $2p$ and N $2p$ mixing defines the shape of the topmost part of the upper valence band. The states near the valence band edge are predominantly N $2p$ states, while the bands in the lower conduction band are mixtures of compa-

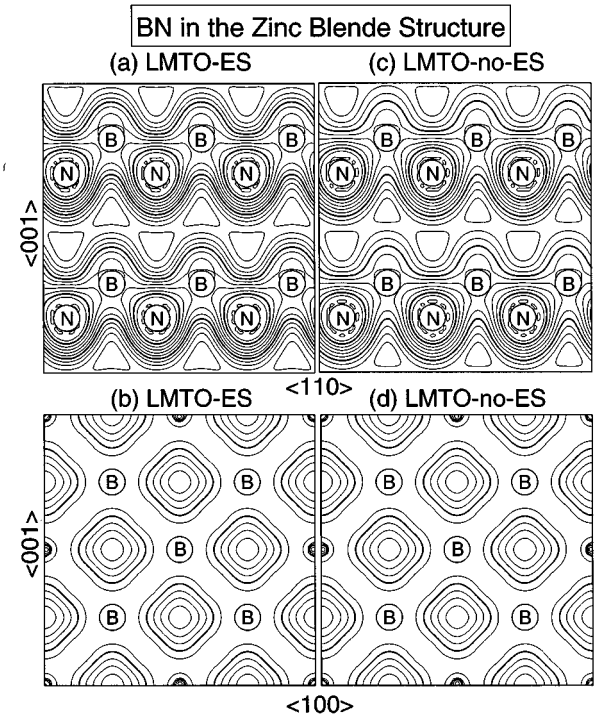

FIG. 3. Total charge density maps calculated using the LMTO-TB method: (a) for the (110) plane (ES calculation); (b) for the (100) plane (ES calculation); (c) for the (110) plane (no ES calculation); and (d) for the (100) plane (no ES calculation). Successive contours differ by $\rho_{n+1}/\rho_n = 1.350$.

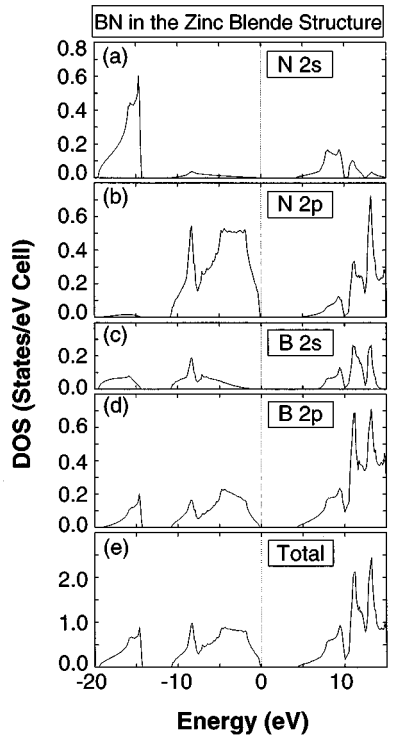

FIG. 4. Total and partial densities of states for c-BN (LMTO-TB-NO-ES calculations).

rable contributions from all antibonding N $2s$, N $2p$, B $2s$, and B $2p$ states, with somewhat larger B $2p$ contributions at the conduction band edge. The inclusion of basis functions up to $l=2$ within the empty spheres appears to be helpful in describing the delocalization of electronic states in the higher energy conduction bands. Results calculated by the FPLAPW, FPLMTO, and LMTO-TB-NO-ES methods are practically identical to the ones presented in Fig. 4. Significant differences occur in an energy range much above the conduction band edge because the characteristic inputs are different in all these computational approaches, and the higher energy conduction band states are sensitive to these computational parameters.

As is well known, LDA calculations provide reliable information for the ground state properties of the crystal, but the energy gaps between the occupied and empty levels are usually underestimated. The experimental band gap found, e.g., from x-ray emission and UV absorption spectra, is in the range 6.0–6.4 eV, as compared with the value of 4.4 eV in our, and other, LDA calculations (Table I). This drawback of the LDA approach can be greatly improved by the computationally intensive GW method[47] (for other approaches see also Refs. 48–51). This quasiparticle treatment has been carried out for c-BN (Ref. 52) and h-BN,[34] with resultant gap values of 6.3 and 5.4 eV, respectively. Since the self-energy of the quasiparticle appears to be only weakly **k** dependent, it is, therefore, justified to use a simpler approach to correct the band gap. We have used the simplified method, LMTO-TB for the band structure calculations, together with the approach of Bechstedt and Del Sole[50] to improve our gap value in c-BN to 6.2 eV.

To close this section, we reiterate that the electronic prop-

erties of ideal c-BN crystal are very reasonably described by the simpler LMTO-ASA-TB-ES method. Therefore, we have used this computationally efficient method to study vacancy states in nonstoichiometric c-BN.

III. BORON AND NITROGEN VACANCIES: GENERAL DISCUSSION

Before discussing the results of our calculations of the electronic structure of the systems with B or N vacancies, it is worthwhile to give a general discussion of what might be expected from considering the crystal structure of zinc-blende structure BN and the atomic properties of boron and nitrogen.

First, consider the B vacancy which is surrounded by four N nearest neighbors, each of which is coordinated with three other occupied B nearest neighbors. Each of these N atoms shares five electrons ($2s^2 2p^3$) with its neighbors leaving, approximately, a total of five ($4\times\frac{5}{4}$) ''dangling,'' unpaired electrons in the vicinity of the B vacancy and its four N nearest neighbors. The unpaired electrons will tend to form bound states with the nitrogen nuclei, starting with a filled s-like state with two electrons (accounting for spin degeneracy), with the next three electrons in a p-like bound state at a higher energy. For the s-like state, the bound state should be close to the location of the N s-like band states, approximately 15 eV below the top of the valence bands in BN, while the p-like state should occur in the valence conduction band gap, e.g., above the upper edge of the N p-like itinerant states. The s-like charge density is expected to be fairly localized around the nitrogen nearest neighbors to the vacancy (since the level is fairly deep in energy), while the p-like states should have characteristic projections toward the B vacancy site.

Similar considerations for the case of an N vacancy give the result that there are three unpaired electrons in the vicinity of the vacancy (from the shared $2s^2 2p^1$ valence electrons of the B nearest neighbors). These three electrons should, with increasing energy, form a doubly occupied s-like state and a partially occupied p-like state. However, in distinction from the case of the B vacancy, the s-like bound state should split off from the top of the valence band since the B s-like states in the crystal (and in the atom) are approximately 10 eV higher in energy than the s-like states for nitrogen forming nonbonding localized states. The p-like bound state should be close to the conduction band edge as it is approximately 5 eV higher in energy in the boron atom. We would expect the s-like charge density in this case to be more diffuse than in the case of the B vacancy due to its falling at a higher energy. We find, as described in the next section, that the p-like state in this case falls as a resonance slightly above the conduction band edge rather than a true bound state. This is a result of the limitations of the LDA, as discussed by Pederson and Klein,[53] and is related to the fact that the LDA potential does not fall off as $1/r$ at large r as should be the case for the ''true'' potential.

We will show in the next section that these physically motivated expectations are borne out by our explicit calculations, although the details of the locations of the bound states and the forms of the charge densities are, of course, dependent on the full response of the crystal to the vacancies and the fact that we are modeling the vacancy with a finite-sized supercell. In particular, a truly isolated vacancy will give an isolated bound state, while, because of the supercell approximation, we will find narrow vacancy bands.

However, the vacancy calculations described below have been done in the LDA approximation since the vacancy-induced gap states we find will not be changed in a qualitative manner (see Ref. 53 for a discussion).

IV. BORON VACANCY IN c-BN

The calculations of the electronic structure of boron vacancies in the zinc-blende phase of BN have been carried out by applying the LMTO-TB-NO-ES method to a 64-atom supercell with the central boron atom replaced by an empty sphere of the same radius (see Sec. II for computational details). Such a model corresponds to the $B_{0.984}N_{1.000}$ stoichiometry of a c-BN crystal.

In order to see how far the states of the vacancy delocalize in the crystal, we have studied the atoms (still remaining at ideal positions) around each vacancy to see how their charge distribution and eigenstates adjust in response to the removal of a nearby atom. The atoms can be categorized by shells: The nearest neighbors to the boron vacancy are N atoms forming the first N shell (1st N shell), the second neighbors constitute the first B shell, the second N and B shells contain, respectively, the third and fourth neighbors, etc. The extent of delocalization can then be examined from the local DOS of each cell. In Fig. 5, we present the total and shell-projected DOS for the atoms up to fourth neighbors. The most striking result of these calculations is the appearance of a narrow and strong ''boron vacancy'' peak split off from the top of the valence band. The gap between the top of the valence band and the ''vacancy level'' is 0.63 eV, and the total width of the vacancy band is 0.45 eV for the system of 64 sites we have studied. The shell-projected DOS show that electronic states at the boron vacancy site consist mainly of p-like states from nitrogen atoms in the 1st N shell. At the same time, the delocalization of boron vacancy states extends to the 2nd N shell, although this contribution is much smaller. Therefore, the origin of the width of this structure can, primarily, be attributed to the formation of molecular-type orbitals from the p-like states of the nearest-neighbor N atoms.

Figure 6(a) gives an expanded view of Fig. 5(a) in the energy range of -5 to 5 eV for the vacancy-related band, which is only partially occupied, with the Fermi energy coinciding with the maximum of the peak in DOS. In other words, a boron vacancy plays the role of a specific acceptor impurity, with the ''impurity level'' being partially occupied already in the ground state (at zero temperature) of the system. At elevated temperatures, electrons can be excited from the valence band to this partially occupied ''vacancy level,'' so that the sample can also exhibit p-doped behavior.

The details of the chemical nature of the boron vacancy can be seen from the partial DOS given in Figs. 6(b)–6(d). The vacancy states are formed from the s-like and p-like states from neighboring N atoms as shown by the DOS structure at about -3 eV (below the top of the valence band). The s component of the vacancy states is completely occupied. The most pronounced contributions are from the nitrogen p

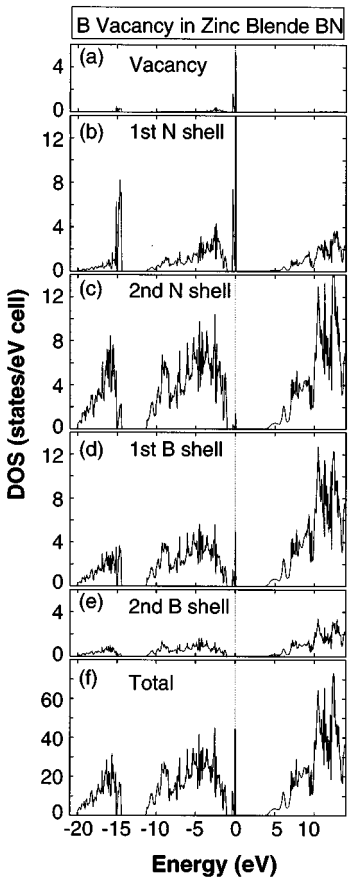

FIG. 5. Shell-projected local densities of states of boron vacany in BN for (a) boron vacancy site; (b) N atoms of the first coordinational sphere (1st N shell with 4 N atoms); (c) N atoms of the third coordinational sphere (2nd N shell with *xx* N atoms); (d) B atoms of the second coordinational sphere (1st B shell with 12 B atoms); (e) B atoms of the fourth coordinational sphere (2nd B shell with *yy* B atoms); and (f) the total DOS.

states of the neighboring atoms. As discussed in the preceding paragraph, they contribute to the states at the Fermi level. Figure 6 shows some *d*-characteristic states contributing to the ''vacancy states.'' This reflects the symmetry of the vacancy site and the surrounding structure on the chemical nature of the vacancy states.

Some qualitative ideas on the charge state of the boron vacancy and its influence on the charge distribution of the atoms nearest to the vacancy site can be drawn from the magnitudes of the charge densities in the atomic spheres given in Table III. It is worth noting that these values refer to some averaged charge gain or loss in the highly overlapping atomic spheres centered at the appropriate atomic sites compared with the value of free-atom charge density in these spheres. By further comparing to the values for the ideal crystal, one can obtain some idea about charge redistribution near the boron vacancy sites in nonstoichiometric *c*-BN crystals. The boron vacancy accumulates negative charge, which is mostly from nitrogen atoms of the 1st N shell. As a result, the 1st N shell atoms, being negatively charged in the ideal crystal, become less ionic. In this sense, a boron vacancy plays the role of a trap for the valence electrons contributed by the nearest-neighbor N atoms. The charges of the second

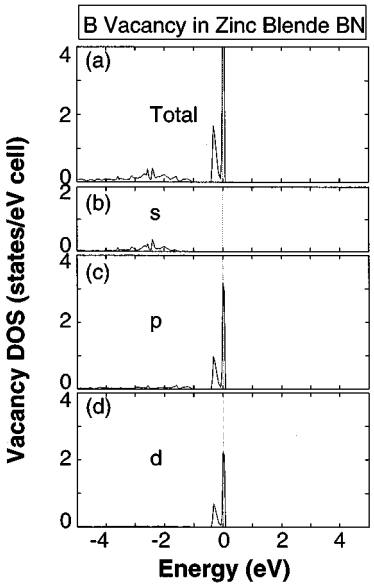

FIG. 6. Partial densities of states for B vacancy: (a) total B vacancy DOS; (b) *s* states; (c) *p* states; (d) *d* states.

up to fourth neighbor atoms are affected by the vacancy to a lesser extent.

These conclusions are confirmed by the charge density plots in the (110) and (100) planes containing the boron vacancy. As is seen from Fig. 7(a), charge distributions of the 1st N shell are deformed and shifted towards the vacancy site compared to the ideal crystal (Fig. 3). The charge density contours in the (100) plane [Fig. 7(b)] show the formation of molecular-type orbitals from the nearest nitrogen neighbors, the 1st N shell atoms, around the boron vacancy.

The charge density plots for the electrons in the vacancy band [the energy interval from -0.5 eV to the Fermi energy in Fig. 6(d)] are given in Fig. 7(c) for the (110) plane and Fig. 7(d) for the (100) plane, respectively. In the (110) plane [Fig. 7(a)], the vacancy states appear to come essentially from the *p* states of the neighboring nitrogen atoms. On the other hand, the contours in the (100) plane [Fig. 7(d)] exhibit *d*-like characteristics reflecting the symmetry around the vacancy. Both plots show the weak extensions of the states to the next shell of boron (the 1st B shell) and nitrogen (the 2nd N shell) atoms.

We conclude in this section that the results of the calculations show (i) a boron vacancy in the *c*-BN crystal behaves as an acceptor-type impurity; (ii) it induces a new, strong, and narrow band of states near the top of the valence band,

TABLE III. Change (relative to the atomic values) of the charge in the atomic spheres in units of $|e|$.

Atom	Ideal BN	B vacancy	N vacancy
B	-0.121	1.302	
N	0.121		0.948
1st coord. sphere		-0.270(N)	-0.474(B)
2nd coord. sphere		-0.118(B)	0.142(N)
3rd coord. sphere		0.127(N)	-0.102(B)
4th coord. sphere		-0.125(B)	0.122(N)

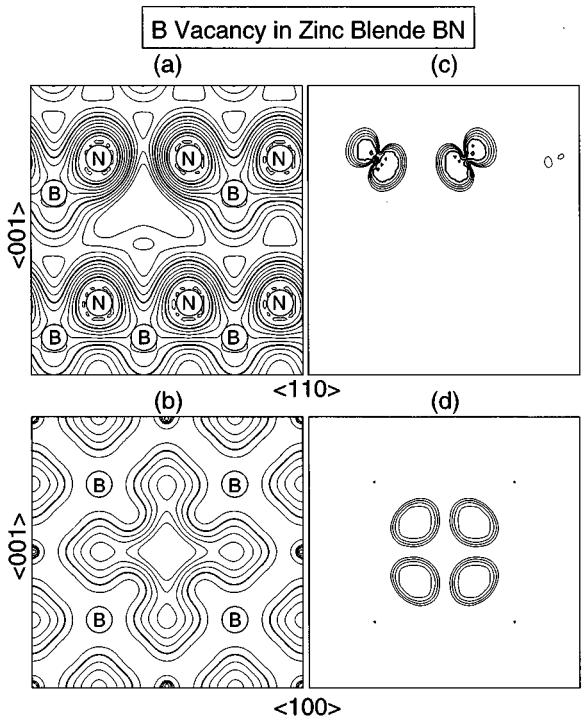

FIG. 7. Charge density maps for a crystal with a B vacancy: (a) ⟨110⟩ plane total valence charge density; (b) ⟨100⟩ boron plane total valence charge density; (c) ⟨110⟩ plane density for the vacancy-induced bands; and (d) ⟨100⟩ boron plane density for the vacancy-induced bands.

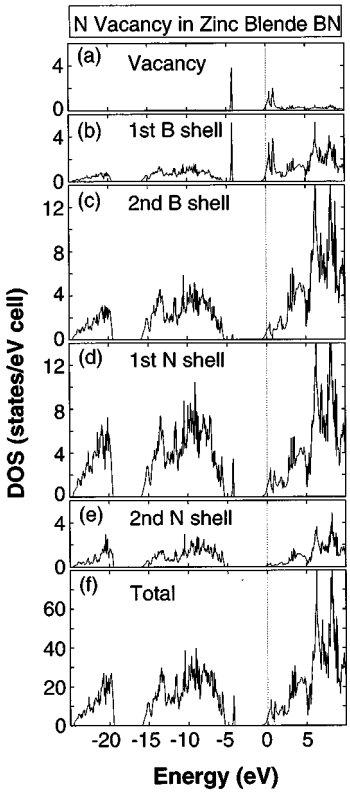

FIG. 8. Shell-projected local densities of states of nitrogen vacany in BN for (a) boron vacancy site; (b) B atoms of the first coordinational sphere (1st N shell with 4 B atoms); (c) B atoms of the third coordinational sphere (2nd N shell with *xx* B atoms); (d) N atoms of the second coordinational sphere (1st B shell with 12 N atoms); (e) N atoms of the fourth coordinational sphere (2nd B shell with *yy* N atoms); and (f) the total DOS.

which reduces the effective band gap value.

V. NITROGEN VACANCY IN *c*-BN

We modeled a nitrogen vacancy in a zinc-blende BN crystal by replacing the central nitrogen atom of the 64-atom supercell by an empty sphere of the same size (with ''vacancy'' *s*, *p*, *d* states included in the basis). Such a model corresponds to the $B_{1.000}N_{0.984}$ stoichiometry of the crystal. The *charge* around the vacancy from *structural unrelaxed* 1st B shell, 1st N shell, and 2nd B shell atoms was allowed to relax and change their electronic states under the influence of the nitrogen vacancy. The LMTO-TB-NO-ES calculation results are presented in Figs. 8–10 and Table III.

A nitrogen vacancy in the BN lattice leads to significant differences for the electronic states and the energy spectrum of the sample as compared to the case of boron vacancy. Although a well-defined peak is split off from the valence band edge similar to the case of the boron vacancy, it is at a somewhat larger separation from the top of the valence band and is now completely occupied. Therefore, the Fermi level is located at the shoulder of the lowest energy peak in the conduction band. From the shell-projected DOS (Fig. 8), it follows that both these structures originate from the interaction of the nitrogen vacancy with the boron atoms in the 1st B shell. Smaller interactions are seen between the vacancy and the nitrogen atoms in the 1st N shell. More distant shells do not make sizable contributions to the formation of the characteristics of the ''vacancy levels'' in the energy spectrum.

The calculated charge in the atomic spheres of atoms in different shells (Table III) shows that the nitrogen vacancy accumulates a lesser amount of electronic charge as compared with the boron vacancy. Most of the charge is originated from the neighboring boron atoms (first B shell). It is interesting to note that nitrogen atoms in the first N shell become more negatively charged than the ones in ideal *c*-BN. Only the atoms of the fourth neighbor (2nd N shell) stop feeling the perturbation induced by the nitrogen vacancy.

The electronic structures of nitrogen vacancy states in the different energy regions can be examined using the partial DOS (Fig. 9). The states split off from the top of the valence band are of *s* symmetry relative to the vacancy site [Fig. 9(a)]. They are related to the *s*-like states of the atoms in the 1st B shell. The *p* states of the vacancy are located at the low energy part of the conduction band [Fig. 9(c)]. The *p* vacancy band overlaps with the low energy conduction states of the ideal *c*-BN crystal rather than splitting off as a bound state below the conduction band edge. As discussed earlier, this is related to a limitation of the LDA. This band comes from the nonbonding *p*-like states of atoms in the 1st B shell.

In Fig. 10, we present the charge density plots for the case of the nitrogen vacancy generated for (110) [Fig. 10(a)] and (100) [Fig. 10(b)] planes, respectively. The charge distribution of 1st B shell atoms appears to be strongly distorted

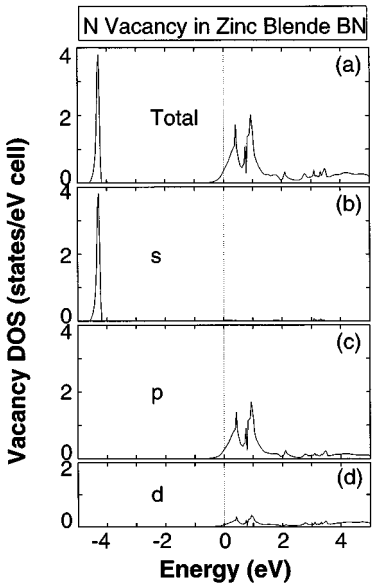

FIG. 9. Densities of states for the N vacancy crystal above the valence band edge (a) total DOS; (b) s-like; (c) p-like; and (d) d-like.

[Fig. 10(a)] near the N vacancy. As compared to the case of boron vacancy [Fig. 7(b)], the localization of the states at the vacancy site [Fig. 10(b)] is much diminished. This strengthens the conclusions made above on the higher degree of charge delocalization near the nitrogen vacancy site as compared with the case of the boron vacancy.

The charge density contours for the s-vacancy and p-vacancy states are given in Figs. 10(d) and 10(c), respectively. The nearly spherical shape of the charge distribution around the vacancy for the s-vacancy band is seen clearly from the contours shown in Fig. 10(d). These states originate from the p orbitals of the nearest boron atoms. Their overlap forms a spherically symmetric molecular-type state. The p-like character of vacancy states near the Fermi level is completely different. As is seen from the charge distributions in the (110) plane [Fig. 10(c)] for the occupied portion of this band, the electronic states of this band are rather delocalized. These states are closely related to the nonbonding sp^3 orbitals from nearby atoms.

VI. SUMMARY

We have presented self-consistent electronic structure calculations for stoichiometric and boron- and nitrogen-deficient zinc-blende boron nitride. The calculations have been performed within the LDA. For c-BN, we used the most precise full-potential LAPW and LMTO methods, and the less accurate LMTO-ASA-TB methods with and without empty spheres. The results of all the methods agree for the band structures, total and partial densities of states, charge density distributions, lattice constants, and bulk modulus. They also show reasonable agreement with the experimental data for cubic BN of nearly stoichiometric compositions, and with previous calculations. These results assure that the simple and flexible LMTO-ASA-TB method can be used to perform model calculations of the electronic structure of vacancies in c-BN.

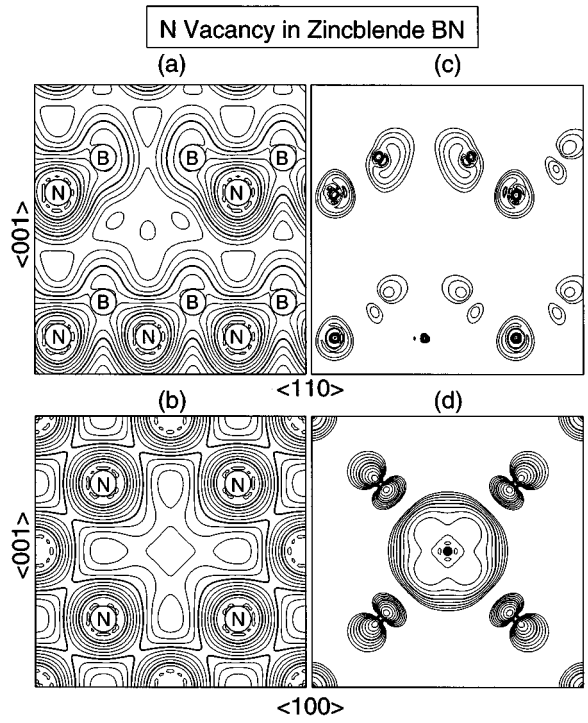

FIG. 10. Charge density maps for a crystal with a N vacancy: (a) $\langle 110 \rangle$ plane total valence charge density; (b) $\langle 100 \rangle$ boron plane total valence charge density; (c) $\langle 110 \rangle$ plane density for the vacancy-induced bands; and (d) $\langle 100 \rangle$ boron plane density for the vacancy-induced bands.

Using a 64-atom supercell, we have studied the electronic states of isolated boron and nitrogen vacancies in zinc-blende boron nitride. Atoms surrounding the vacancy remain at ideal positions. Both vacancy types cannot be considered as isolated point defects as they induce perturbations which are not completely localized at the vacancy sites. The range of interactions is at least extended to second nearest neighbors. The delocalization effects of the electronic states are stronger in the case of boron vacancy.

Both boron and nitrogen vacancies induce localized narrow ''vacancy bands'' in the energy gap region of stoichiometric c-BN. The boron-related vacancy band has a 0.4-eV width and is split off from the top of the valence band at an energy of 0.6 eV above the edge. This band is partially occupied and can play the role of exhibiting p-type doping behavior for c-BN when the valence electrons are thermally excited to this band. Creation of a nitrogen vacancy results in the appearance of two narrow N vacancy-related bands: (i) a completely occupied s-type band split off from the top of the valence band, and (ii) a partially occupied delocalized p-type band, which overlaps the conduction band edge. It is likely that the overlap is caused by the inadequacy of the LDA. However, our results suggest that the nitrogen vacancy can provide electrons ionized thermally to the conduction band and can play the role of an effective donor impurity, which increase the n-type conductivity of the crystal.

The charge density plots and the shell- and orbital-projected DOS for nonstoichiometric c-BN crystals give detailed information on the nature of the vacancy-related states. These calculations provide detailed information on the elec-

tronic states of isolated boron and nitrogen vacancies in zinc-blende boron nitride.

ACKNOWLEDGMENTS

We thank Dr. A. Chaiken and Dr. L. J. Terminello of Lawrence Livermore National Laboratory for stimulating our interest in this problem and valuable discussions, and Dr. M. van Schilfgaarde for consultations on the computational details of the FPLMTO method. B.M.K. and Z.W.L. acknowledge research support from the University of California. The computational facilities were provided by a grant from the NSF San Diego Supercomputing Center.

[1] *Diamond, Silicon Carbide and Related Wide Bandgap Semiconductors*, edited by J. T. Glass, R. Messmer, and N. Fujimori, MRS Symposia Proceedings No. 162 (Materials Research Society, Pittsburgh, PA, 1990).
[2] R. F. Davis, Z. Sitar, B. E. Williams, H. S. Kong, H. J. Kim, J. W. Palmour, J. A. Edmond, J. Ryu, J. T. Glass, and C. H. Carter, Jr., Mater. Sci. Eng. B **1**, 77 (1988).
[3] J. H. Edgar, J. Mater. Res. **7**, 235 (1992).
[4] R. Riedel, Adv. Mater. **6**, 549 (1994).
[5] R. T. Paine and C. K. Narula, Chem. Rev. **90**, 73 (1990).
[6] E. Yamaguchi, Mater. Sci. Forum **54-55**, 329 (1990).
[7] V. L. Solozhenko, G. Will, H. Hupen, and F. Elf, Solid State Commun. **90**, 65 (1994).
[8] T. Sato, Proc. Jpn. Acad. Ser. B **61**, 459 (1985).
[9] P. Lin, C. Deshpandey, H. J. Doerr, R. F. Bunshah, K. L. Chorpa, and V. Vankar, Thin Solid Films **153**, 487 (1987).
[10] B. Rother and C. Weissmantel, Phys. Status Solidi A **87**, K119 (1985).
[11] G. Mandel, F. F. Morehead, and P. R. Wagner, Phys. Rev. A **136**, 826 (1964).
[12] O. Mishima, Mater. Sci. Forum **54-55**, 313 (1990); O. Mishima *et al.*, in *Electroluminescence*, edited by S. Shionoya and H. Kobayashi (Springer-Verlag, Berlin, 1989), p. 386.
[13] H. Saitoh, T. Hirose, H. Matsui, Y. Hirotsu, and Y. Ichinose, Surf. Coat. Technol. **39/40**, 265 (1989).
[14] T. Andoh, S. Nishiyama, H. Kirimura, T. Mikami, K. Ogata, and F. Fujumoto, Nucl. Instrum. Methods B **56/60**, 276 (1991).
[15] M. Murakawa and S. Watanabe, Surf. Coat. Technol. **43/44**, 128 (1990).
[16] D. J. Kester and R. Messier, J. Appl. Phys. **72**, 504 (1992).
[17] A. Chayahara, H. Yokoyama, T. Imura, and Y. Osaka, Jpn. J. Appl. Phys. **26**, L1435 (1987).
[18] H. Saitoh and W. A. Yarbrough, Appl. Phys. Lett. **58**, 2482 (1991).
[19] A. Bath, O. Baehr, M. Barrada, B. Lepley, P. J. van der Put, and J. Schoonman, Thin Solid Films **241**, 278 (1994).
[20] G. L. Doll, J. A. Sell, C. A. Taylor II, and R. Clarke, Phys. Rev. B **43**, 6816 (1991).
[21] M. Mieno and T. Yoshida, Jpn. J. Appl. Sci. **29**, L1175 (1990).
[22] A. L. Ballal, L. Slamanca Riba, G. L. Doll, C. A. Taylor II, and R. Clarke, J. Mater. Res. **7**, 1618 (1992).
[23] O. Burat, D. Boucher, V. Stambouli, and G. Gautherin, J. Appl. Phys. **68**, 2780 (1990).
[24] M. Lu, A. Bosetta, R. Sukach, A. Bensaoula, K. Walters, K. Eipers-Smith, and A. Schultz, Appl. Phys. Lett. **64**, 1514 (1994).
[25] N. Tanabe and M. Iwaki, Nucl. Instrum. Methods **80/81**, 1349 (1993).
[26] L. J. Terminello, A. Chaiken, D. A. Lapiano-Smith, G. L. Doll, and T. Sato, J. Vac. Sci. Technol. A **12**, 2462 (1994).
[27] M. D. Wiggins, C. R. Aita, and F. S. Hickernell, J. Vac. Sci. Technol. A **2**, 322 (1984).
[28] E. J. Andrey, A. Katzir, and J. T. Russ, Phys. Rev. B **13**, 2831 (1976).
[29] M. B. Khudisman, V. S. Nespor, and L. I. Feldgin, Izv. Akad. Nauk SSSR, Neorg. Mater. **22**, 694 (1986) [Inorg. Mater. (USSR) **22**, 611 (1986)].
[30] A. M. Dorbotvorski and R. A. Evarestov, Phys. Status Solidi B **66**, 83 (1974).
[31] V. V. Lopatin and F.V. Konusov, J. Phys. Chem. Solids **53**, 847 (1992).
[32] K. T. Park, K. Terakura, and N. Hamada, J. Phys. C **20**, 1241 (1987).
[33] N. E. Christensen and I. Gorczyca, Phys. Rev. B **50**, 4397 (1994).
[34] X. Blase, A. Rubio, S. G. Louie, and M. Cohen, Phys. Rev. B **52**, 2225 (1995).
[35] P. Hohenberg and W. Kohn, Phys. Rev. **136**, B864 (1964); W. Kohn and L. J. Sham, *ibid.* **140**, A1133 (1965).
[36] O. K. Anderson, Phys. Rev. B **12**, 3060 (1975).
[37] D. J. Singh, *Planewaves, Pseudopotentials, and the LAPW Method* (Kluwer, Boston, 1994).
[38] M. Methfessel, Phys. Rev. B **38**, 1537 (1988).
[39] O. K. Andersen and O. Jepsen, Phys. Rev. Lett. **53**, 2571 (1984).
[40] M. van Schilfgaarde, T. A. Paxton, O. Jepsen, and O. K. Anderson, TB-LMTO PROGRAM-VERSION 44, Max Planck Institute for Solid State Physics, 1994.
[41] L. Hedin and B. I. Lundqvist, J. Phys. C **4**, 2064 (1971).
[42] R. W. G. Wyckoff, *Crystal Structures*, 2nd ed. (Interscience, New York, 1963); *International Tables for X-ray Crystallography* (Kynoch Press, Birmingham, 1974).
[43] H. J. Monkhorst and J. D. Pack, Phys. Rev. B **13**, 5188 (1976).
[44] R. M. Wentzcovitch, K. J. Chang, and M. L. Cohen, Phys. Rev. B **34**, 1071 (1986).
[45] V. A. Fomichev and M. A. Rumsh, J. Chem. Phys. **48**, 555 (1968).
[46] J. Hosoi, T. Oikawa, M. Inoue, Y. Masui, and T. Endo, J. Electron. Spectrosc. Relat. Phenom. **27**, 243 (1982).
[47] V. Fiorentini, M. Methfessel, and M. Scheffler, Phys. Rev. B **47**, 13 353 (1993).
[48] W. Lu, K. Zhang, and X. Xie, J. Phys. C **5**, 875 (1993).
[49] K. Kobayashi, T. Sano, and Y. J. I'Haya, Chem. Phys. Lett. **219**, 53 (1994).
[50] F. Bechstedt and R. Del Sole, Phys. Rev. B **38**, 7710 (1988).
[51] S. J. Jenkins, G. P. Srivastava, and J. C. Inkson, J. Phys. Condens. Matter **6**, 8781 (1994).
[52] M. P. Surh, S. G. Louie, and M. L. Cohen, Phys. Rev. B **43**, 9126 (1991).
[53] M. R. Pederson and B. M. Klein, Phys. Rev. B **37**, 10 319 (1988).